Phase transitions in a chiral model of nuclear matter

Nguyen Tuan Anh[1] and Dinh Thanh Tam[2,3]
[1]*Electric Power University, 235 Hoang Quoc Viet, Hanoi, Vietnam*
[2]*University of Taybac, Sonla, Vietnam*
[3]*Vietnam Atomic Energy Commission, 59 Ly Thuong Kiet, Hanoi, Vietnam*
(Received 11 October 2011; published 29 December 2011)

The phase structure of symmetric nuclear matter in the extended Nambu–Jona-Lasinio (ENJL) model at finite baryon chemical potential μ_B and temperature T is studied by means of the effective potential in the one-loop approximation. It is found that chiral symmetry gets restored at high nuclear density and a typical first-order phase transition between liquid and gas occurs at zero temperature, $T = 0$, which weakens as T grows and eventually ends up with a critical point at $T \lesssim 18$ MeV. This phase transition scenario is confirmed by investigating the evolution of the effective potential as a function of effective nucleon mass and the equation of state. The restoration of chiral symmetry gives a second-order phase transition in the region $0 \leqslant T \lesssim 171$ MeV and a first-order transition in the region $T \gtrsim 171$ MeV.

DOI: 10.1103/PhysRevC.84.064326 PACS number(s): 11.30.Rd, 05.70.Fh, 21.65.−f

I. INTRODUCTION

Presently, heavy-ion collisions at high energies provide the opportunity to explore many interesting properties of matter under extreme conditions. In this connection, properties of hot and dense strongly interacting matter, especially its chiral transitions, are in the focus of experimental and theoretical investigations. There has been considerable progress in exploring the chiral phase transition in quark matter within the framework of lattice QCD simulation [1] and effective QCD models [2,3]. Simulations [4] on the lattice including dynamical quarks with realistic masses predict a crossover-like deconfinement (chiral) transition at temperatures around 170 MeV. The situation at finite baryon densities remains uncertain and subject to model building.

In fact, the phase transition of nuclear matter has been often studied using numerous phenomenological models providing descriptions in terms of nucleonic degrees of freedom [5–15]. Nonrelativistic nuclear models using various types of nucleon-nucleon potentials are available at low density exclusively, but they fail to reflect the physical characteristics of dense matter. Relativistic mean-field nuclear models of the Walecka type [16] have successfully reproduced many physical properties of medium and heavy nuclei. Other relativistic nuclear models have been developed and have obtained important results. However, all preceding models share the serious drawback of not respecting chiral symmetry, which is commonly accepted as one of the basic symmetries of the strong interaction. The chiral phase transition in a dense matter state plays a crucial role in the study of physical properties of excited nuclei as well as of the structure of compact stars and the evolution of the early universe.

There exist several chiral models which could potentially be used for describing nuclear matter. Most popular are the Nambu–Jona-Lasinio (NJL) model [17] and the linear σ model [18]. They are able to explain spontaneous breaking of chiral symmetry in vacuum and its restoration at high energy densities. But the simplest versions of these models fail to reproduce nuclear saturation properties. In particular, the linear σ model predicts only an abnormal state of nuclear matter [19] where the chiral symmetry is restored and nucleons have vanishing effective mass. Several more sophisticated models of this kind have been suggested [20–24]. Although they are able to reproduce the nuclear ground state, new problems appear within these models; in particular, some of them do not predict restoration of chiral symmetry at high baryon densities. There were also attempts to use the NJL model to describe cold nuclear matter [25–27]. It has been argued [25,26] that bound nucleonic matter with spontaneously broken chiral symmetry is not possible within the standard NJL. The authors of Ref. [25] suggested including additional scalar-vector interaction terms to reproduce the observed saturation properties of nuclear matter. On the other hand, it has been shown [27] that by assuming a sufficiently low value of the cutoff momentum ($\Lambda \simeq 0.3$ GeV) it is possible to produce a bound state at normal density even in the standard NJL model. However, in this case the nucleon effective mass at $\rho_B = \rho_0$ is predicted twice as small as its empirical value.

Recently, we reconsidered the possibility of using an extended version of the NJL model including in addition a scalar-vector interaction in order to describe nuclear matter at finite temperature and the phase structure of the liquid-gas transition [28]. This ENJL version reproduces well the observed saturation properties of nuclear matter such as equilibrium density, binding energy, compression modulus, and nucleon effective mass at $\rho_B = \rho_0$. It reveals a first-order phase transition (of the liquid-gas type) occurring at subsaturated densities; such a transition is present in any realistic model of nuclear matter; However, the model predicts an only approximate restoration of chiral symmetry at high baryon densities, $\rho_B \gtrsim 3\rho_0$, and does not exhibit any certain chiral phase transition.

As discussed in Ref. [14], a model that may suit well our purpose is the extended Nambu–Jona-Lasinio (ENJL) model. In the present paper, we consider its phase structures [28] in the case of exact chiral symmetry. The certain chiral transition is studied in addition to the saturation properties of nuclear

matter and the consistency of the nucleon effective mass and incompressibility with their experimental values. Our model is able to describe simultaneously the saturation properties of nuclear matter (liquid-gas transition) and the restoration of chiral symmetry at high baryon densities (chiral transition). We start from the Lagrangian

$$\begin{aligned}\mathcal{L} &= \mathcal{L}_{\text{NJL}} + \mu\bar{\psi}\gamma_0\psi,\\ \mathcal{L}_{\text{NJL}} &= \bar{\psi}i\partial\!\!\!/\psi + \frac{G_s}{2}[(\bar{\psi}\psi)^2 + (\bar{\psi}i\gamma_5\vec{\tau}\psi)^2]\\ &\quad - \frac{G_v}{2}[(\bar{\psi}\gamma^\mu\psi)^2 + (\bar{\psi}\gamma_5\gamma^\mu\psi)^2] + \frac{G_{sv}}{2}[(\bar{\psi}\psi)^2\\ &\quad + (\bar{\psi}i\gamma_5\vec{\tau}\psi)^2][(\bar{\psi}\gamma^\mu\psi)^2 + (\bar{\psi}\gamma_5\gamma^\mu\psi)^2], \qquad (1)\end{aligned}$$

where μ is the baryon chemical potential, τ is the isospin Pauli matrices, and G_s, G_v, and G_{sv} are coupling constants.

One of the main aims of the paper is to test the validity of the above chiral ENJL Lagrangian (1): namely, whether or not it reproduces the well-established results for symmetric nuclear matter, such as the value of the in-medium nucleon mass, the value of incompressibility and the liquid-gas phase transition at subsaturation density, $\rho < \rho_0 \approx 0.17$ fm^{-3}. Therefore, in what follows, we deal only with symmetric nuclear matter ($\mu_I = 0$).

In the mean-field approximation we replace

$$\begin{aligned}(\bar{\psi}\Gamma_i\psi)^2 &\simeq 2\bar{\psi}\Gamma_i\psi\langle\bar{\psi}\Gamma_i\psi\rangle - \langle\bar{\psi}\Gamma_i\psi\rangle^2,\\ (\bar{\psi}\Gamma_i\psi\bar{\psi}\Gamma_j\psi)^2 &\simeq \langle\bar{\psi}\Gamma_i\psi\rangle^2(2\bar{\psi}\Gamma_j\psi\langle\bar{\psi}\Gamma_j\psi\rangle)\\ &\quad + (2\bar{\psi}\Gamma_i\psi\langle\bar{\psi}\Gamma_i\psi\rangle)\langle\bar{\psi}\Gamma_j\psi\rangle^2\\ &\quad - 3\langle\bar{\psi}\Gamma_i\psi\rangle^2\langle\bar{\psi}\Gamma_j\psi\rangle^2 \qquad (2)\end{aligned}$$

with $\Gamma = \{1, i\gamma_5\vec{\tau}, \gamma_\mu, \gamma_5\gamma_\mu\}$, where the angular brackets mean averaging at finite density and temperature.

Relations (2) combine with bosonization

$$\boldsymbol{\sigma} = \bar{\psi}\psi, \quad \vec{\boldsymbol{\pi}} = \bar{\psi}i\gamma_5\vec{\tau}\psi, \quad \boldsymbol{\omega}_\mu = \bar{\psi}\gamma_\mu\psi, \quad \boldsymbol{\phi}_\mu = \bar{\psi}\gamma_5\gamma_\mu\psi,$$

yielding

$$\begin{aligned}\mathcal{L} &= \bar{\psi}(i\partial\!\!\!/ + \gamma_0\mu)\psi + [G_s + G_{sv}(\boldsymbol{\omega}^2 + \boldsymbol{\phi}^2)]\bar{\psi}(\boldsymbol{\sigma} + i\gamma_5\vec{\tau}\vec{\boldsymbol{\pi}})\psi\\ &\quad - [G_v - G_{sv}(\boldsymbol{\sigma}^2 + \boldsymbol{\pi}^2)]\bar{\psi}\gamma^\mu(\boldsymbol{\omega}_\mu + \gamma_5\boldsymbol{\phi}_\mu)\psi\\ &\quad - \frac{G_s}{2}(\boldsymbol{\sigma}^2 + \boldsymbol{\pi}^2) + \frac{G_v}{2}(\boldsymbol{\omega}^2 + \boldsymbol{\phi}^2)\\ &\quad - 3\frac{G_{sv}}{2}(\boldsymbol{\sigma}^2 + \boldsymbol{\pi}^2)(\boldsymbol{\omega}^2 + \boldsymbol{\phi}^2). \qquad (3)\end{aligned}$$

The structure of the paper is as follows. Section II presents the equations of state of chiral nuclear matter for later use. Section III determines the static properties of symmetric nuclear matter at zero temperature. Section IV studies the phase transitions of chiral nuclear matter. Conclusions and perspectives are presented in Sec. V.

II. EQUATIONS OF STATE

At $\mu_I = 0$, the σ, π, ω, and ϕ fields have the ground state expectation values

$$\langle\boldsymbol{\sigma}\rangle = u, \quad \langle\boldsymbol{\pi}_i\rangle = 0, \quad \langle\boldsymbol{\omega}_\mu\rangle = \rho_B\delta_{0\mu}, \quad \langle\boldsymbol{\phi}_\mu\rangle = 0 \qquad (4)$$

in cold nuclear matter. Inserting Eq. (4) into Eq. (3) we obtain

$$\mathcal{L}_{\text{MFT}} = \bar{\psi}(i\partial\!\!\!/ - M^* + \gamma_0\mu^*)\psi - U(\rho_B, u), \qquad (5)$$

where

$$M^* = -\tilde{G}_s u, \qquad (6)$$

$$\mu^* = \mu_B - \Sigma_v = \mu_B - (G_v - G_{sv}u^2)\rho_B, \qquad (7)$$

$$U(\rho_B, u) = \tfrac{1}{2}\big(G_s u^2 - G_v\rho_B^2 + 3G_{sv}u^2\rho_B^2\big), \qquad (8)$$

with

$$\tilde{G}_s = G_s + G_{sv}\rho_B^2 = G_s[1 + \alpha(\rho_B/\rho_0)^2], \quad \alpha = \rho_0^2 G_{sv}/G_s.$$

The solution M^* of Eq. (6) is the nucleon effective mass, which reduces to the nucleon mass in vacuum.

Starting from Eq. (5) we establish the partition function

$$Z = \int D\bar{\psi}\,D\psi\,D\sigma\,D\vec{\pi}\,D\omega_\mu\ \exp\int_0^\beta d\tau\int_V d^3x\ \mathcal{L}_{\text{MFT}}.$$

Integrating out the nucleon degrees of freedom gives

$$Z = \exp\left(-\frac{VU}{T}\right)\det S^{-1}, \qquad (9)$$

with

$$S^{-1}(k) = \hat{k} - M^* + \gamma_0\mu^*,$$

giving

$$\det S^{-1}(k) = (k_0 - E_-)(k_0 + E_+), \qquad (10)$$

in which

$$E_\mp = E_k \mp \mu^*, \quad E_k = \sqrt{k^2 + M^{*2}}.$$

Based on Eqs. (9) and (10) the effective potential is derived immediately:

$$\begin{aligned}\Omega &= -\frac{T}{V}\ln Z = U(\rho_B, \rho_s) + i\,\text{Tr}\ln S^{-1}\\ &= U(\rho_B, u) + 2N_f\int\frac{d^3k}{(2\pi)^3}[E_k + T\ln(n_-n_+)], \qquad (11)\end{aligned}$$

where $n_\mp = [e^{E_\mp/T} + 1]^{-1}$ and $N_f = 2$ for nuclear matter and $N_f = 1$ for neutron matter.

The pressure P is defined as

$$P = -\Omega_{\min}.$$

The energy density is obtained by taking the Legendre transform of P

$$\begin{aligned}\mathcal{E} &= \Omega + T\varsigma + \mu_B\rho_B\\ &= U(\rho_B, u) + 2N_f\int\frac{d^3k}{(2\pi)^3}\Sigma_v(n_- - n_+)\\ &\quad + 2N_f\int\frac{d^3k}{(2\pi)^3}E_k(n_- + n_+ - 1), \qquad (12)\end{aligned}$$

with the entropy density defined by

$$\begin{aligned}\varsigma &= -2N_f\int\frac{d^3k}{(2\pi)^3}[n_-\ln n_- + (1 - n_-)\ln(1 - n_-)\\ &\quad + n_+\ln n_+ + (1 - n_+)\ln(1 - n_+)]. \qquad (13)\end{aligned}$$

The ground state of nuclear matter is determined by the minimum condition

$$\frac{\partial \Omega}{\partial u} = 0,$$

or

$$u = \rho_s = 2N_f \int \frac{d^3k}{(2\pi)^3} \frac{M^*}{E_k}(n_- + n_+ - 1), \tag{14a}$$

which is usually called the gap equation.

In terms of the baryon density

$$\rho_B = \frac{\partial P}{\partial \mu_B} = 2N_f \int \frac{d^3k}{(2\pi)^3}(n_- - n_+), \tag{14b}$$

the expression for P reads

$$P = -\frac{(m_0 - M^*)^2}{2\tilde{G}_s} - \frac{G_v}{2}\rho_B^2 + (\mu_B - \mu^*)\rho_B - 2N_f \int \frac{d^3k}{(2\pi)^3}[E_k + T\ln(n_- n_+)], \tag{15}$$

and the energy density takes the form

$$\mathcal{E} = \frac{(m_0 - M^*)^2}{2\tilde{G}_s} + \frac{G_v}{2}\rho_B^2 + 2N_f \int \frac{d^3k}{(2\pi)^3} E_k(n_- + n_+ - 1). \tag{16}$$

Equations (15) and (16) are the equations of state which govern all the phase transition processes of nuclear matter.

III. SATURATION PROPERTIES

At zero temperature Eqs. (14a), (14b), (15), and (16) simplify:

$$u = -\frac{N_f}{\pi^2}\int_{k_F}^{\Lambda} k^2 dk \, \frac{M^*}{(k^2 + M^{*2})^{1/2}}, \tag{17}$$

$$\rho_B = N_f \frac{k_F^3}{3\pi^2}, \tag{18}$$

$$\mathcal{E} = \frac{(m_0 - M^*)^2}{2\tilde{G}_s} + \frac{G_v}{2}\rho_B^2 - \frac{N_f}{\pi^2}\int_{k_F}^{\Lambda} k^2 dk \, (k^2 + M^{*2})^{1/2}. \tag{19}$$

We use the method developed in Ref. [14] to determine the four parameters G_s, G_v, α, and Λ for symmetric nuclear matter; it is based on requiring that a constraint be obeyed together with the saturation condition:

(i) As, in vacuum, $\rho_B = 0$, we must have $M^* = M_N$ with $M_N = 939$ MeV, the nucleon mass in vacuum. Consequently, Eq. (6) provides the first constraint

$$M_N = -\tilde{G}_s u_{\rm vac}, \tag{20}$$

with $u_{\rm vac}$ satisfying the gap equation (17) taken at $\rho_B = 0$ (i.e., $k_F = 0$).

(ii) The saturation mechanism requires that the binding energy

$$\mathcal{E}_{\rm bin} = -M_N + \mathcal{E}/\rho_B \tag{21}$$

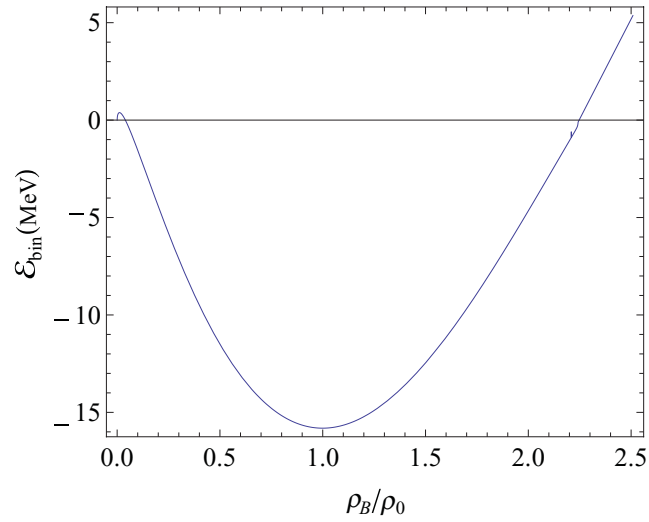

FIG. 1. (Color online) Nuclear binding energy as a function of baryon density.

reaches its minimal value

$$(\mathcal{E}_{\rm bin})_{\rho_0} \simeq -15.8\text{MeV},$$

at normal density $\rho_B = \rho_0 \simeq 0.17$ fm^{-3}, where $\mathcal{E}$ is given by Eq. (19).

The numerical computation shows that $G_s = 8.8975$ fm^2, $G_v/G_s = 0.9485$, $\alpha = 0.031$, and $\Lambda = 400$ MeV. Figure 1 displays the dependence of the binding energy on baryon density. Next, using these values, we calculate the in-medium nucleon mass,

$$M^*/M_N \simeq 0.6633,$$

and the incompressibility

$$K_0 = 9\rho_0^2\left(\frac{\partial^2 \mathcal{E}_{\rm bin}}{\partial \rho_B^2}\right)_{\rho_0} \simeq 276.23 \text{ MeV}.$$

An analysis [29] has shown that such an incompressibility may be more compatible with the data than that previously reported [30], $K_0 = 180$–240 MeV.

At this stage, we have therefore successfully obtained the values of two key nuclear quantities, which are in good agreement with those widely accepted in the literature [31].

Table I lists all the calculated values for parameters and physical quantities concerned.

The above values are adopted as input parameters to our model; we are now in a position to study the phase transitions numerically.

TABLE I. Values of parameters and physical quantities.

	Λ(GeV)	G_s(fm^2)	G_v/G_s	m_0	α	M^*/M_N	K_0(MeV)
[28]	0.4	8.507	0.933	41.26	0.032	0.684	285.91
Here	0.4	8.897	0.949		0.031	0.663	267.23

IV. PHASE STRUCTURE

In our chiral nuclear model, in addition to the usual liquid-gas nuclear phase transition, a chiral restoration phase transition occurs at high nuclear density and/or high temperature. This is one of the fundamental issues of any chiral model of strongly interacting matter. Therefore, both types of phase transitions are presented below in succession.

A. Liquid-gas phase transition at subsaturation density

It is necessary to prove that the theory must exhibit a liquid-gas phase transition at subsaturation density and zero temperature, a well known fact in nuclear physics. To do this, we first solve numerically the gap equation for a chiral condensate (14a) and obtain in Fig. 2 the evolution of a chiral condensate as a function of μ_B for various values of T. It is clear that chiral symmetry gets restored at large μ_B and, moreover, for $T > 18$ MeV the order parameter u is a single-valued function of the baryon chemical potential μ_B and tends slowly toward zero. This kind of behavior is usually defined as a crossover transition. Meanwhile, for lower T, $0 \leqslant T \lesssim 18$ MeV, the order parameter turns out to be a multivalued function of μ_B, where, according to Askawa and Yazaki [2], a first-order phase transition occurs. Then applying the method proposed in Ref. [2], we obtain the phase diagram displayed in Fig. 3. It displays a clear liquid-gas transition. Here the solid line denotes a first-order phase transition ending up with a critical end point, CEP ($T \simeq 18$ MeV, $\mu_B \simeq 922$ MeV). This is precisely the liquid-gas phase transition of symmetric nuclear matter at subsaturation. Figure 3 is in good agreement with the conjectured QCD phase diagram [32]. Low-energy heavy-ion collisions experiments indicate that $\mu_{\rm CEP} \sim 923$ MeV, $T_{\rm CEP} =$ 15–20 MeV [33].

The above result is also visible on the dependence of the effective potential on M^* for several values of T. As shown in Fig. 4, for $T \lesssim 18$ MeV the first-order phase transition displays two minima corresponding to phases of restored and broken symmetries separated by a barrier. As T increases further, these minima fade away and at $T \simeq 18$ MeV the barrier disappears, signaling the onset of a crossover phase transition. The effect shows up clearly on the equation of state, as illustrated in Fig. 5 where isotherms are seen to display typical van der Waals shapes. Such structures are reminiscent of those derived from a number of nuclear models [34,35] depending on the effective forces chosen, such as the Skyrme effective interaction and

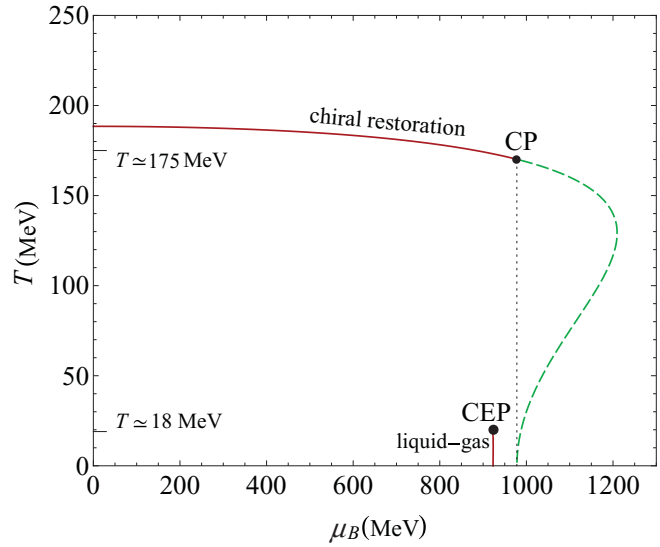

FIG. 3. (Color online) The phase transitions of the chiral nuclear matter in the (T, μ_B) plane. The solid line means a first-order phase transition. CEP ($T = 18$ MeV, $\mu_B = 922$ MeV) is the critical end point. The dashed line denotes a second-order transition. CP ($T =$ 171 MeV, $\mu_B = 980$ MeV) is the tricritical point, where the line of first-order chiral phase transition meets the line of second-order phase transition.

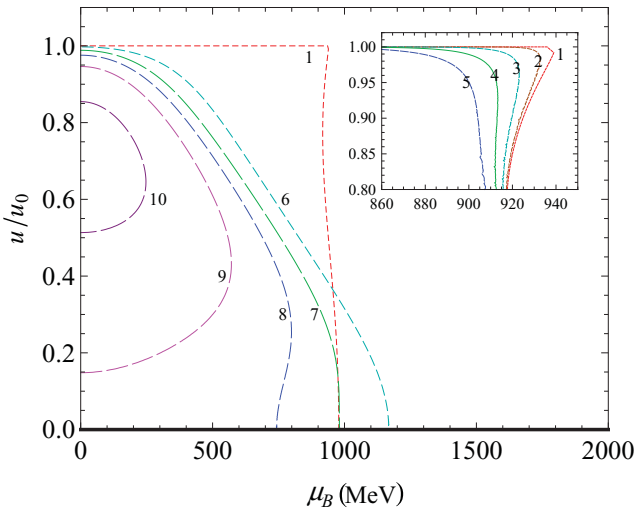

FIG. 2. (Color online) The evolution of a chiral condensate u vs μ_B at various values of T. From the right the graphs correspond to $T = 0$, 150, 170, 180, 190, 200 MeV, respectively. The inset shows $u(T, \mu_B)$ at the low values of T, $T = 0$ (line 1), 5 MeV (line 2), 10 MeV (line 3), 15 MeV (line 4), and 20 MeV (line 5).

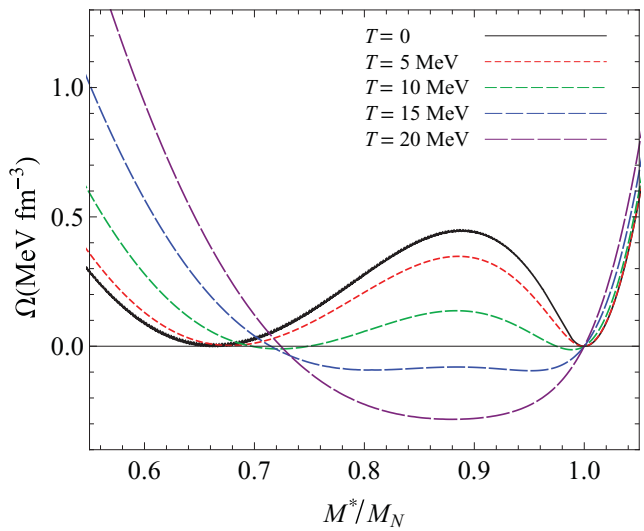

FIG. 4. (Color online) The evolution of effective potential vs M^* at several values of T and μ_B in the region of liquid-gas phase transition.

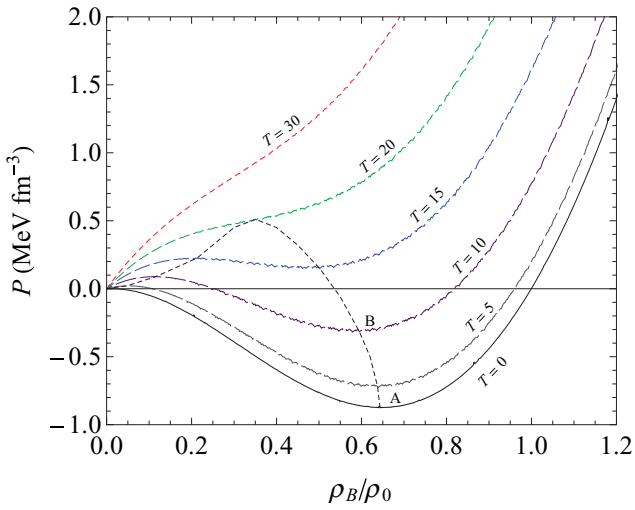

FIG. 5. (Color online) The EoS for several temperature steps. ABO is the spinodal line.

finite temperature Hartree-Fock model [34]. The line AB is part of the spinodal line that delimits the instability condition,

$$\left(\frac{\partial P}{\partial \rho_B}\right)_T < 0.$$

The isotherm segments having negative pressures and obeying the above condition correspond to metastable states [36]. Figure 5 indicates that the phase transition occurs at a critical point $\rho_c \sim 0.3$–$0.4\rho_0$ for $T_c \sim 16$–18 MeV, in agreement with other predictions [37].

Additional insight is obtained from the study of the equation of state at high densities and zero temperature. Figure 6 shows the zero-temperature equation of state for symmetric nuclear matter; the shaded region corresponds to the constraint imposed on the high-density behavior of the pressure from

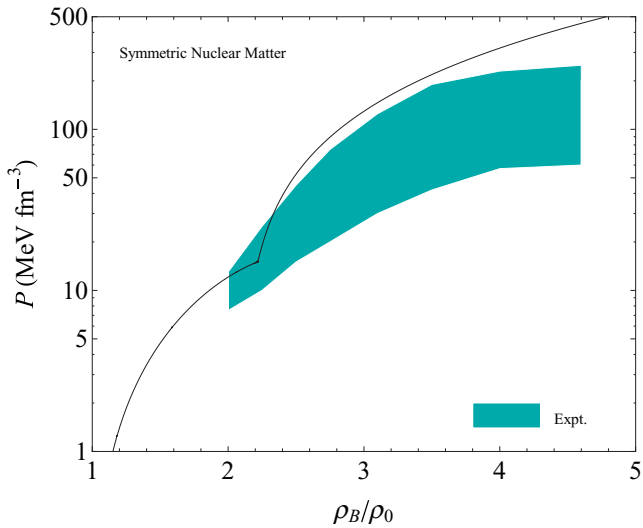

FIG. 6. (Color online) The EoS of cold symmetric nuclear matter at high baryon density. The shaded area denotes constraint on the high-density behavior of pressure consistent with the experimental flow data [38].

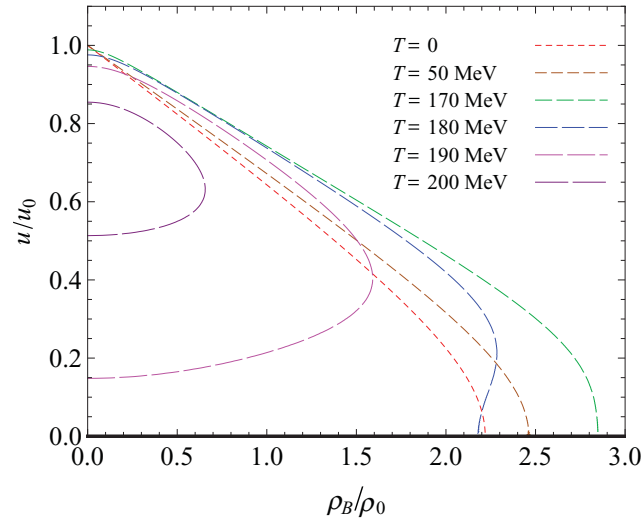

FIG. 7. (Color online) The ρ_B dependence of chiral condensate at various values of T.

simulations of flow data deduced from heavy-ion collision experiments [38].

B. Chiral phase transition

The study of the chiral phase transition is well known to be a difficult problem. As mentioned in Ref. [39], the smooth dependence of chiral condensates as a function of temperature or density has lead several authors to believe that the phase transition is second order. We adopt the method developed by Askawa and Yazaki [2] which is commonly accepted as being well adapted to our purpose. We evaluate numerically the dependence of the chiral condensate on density at various values of T from the gap equation (14a). The result, shown in Fig. 7, shows the existence of two T regions corresponding to different behaviors of the chiral condensate.

For $0 \leqslant T \lesssim 171$ MeV, the order parameter u tends to zero and is a single-valued function of ρ_B, characteristic of a second-order phase transition as defined by Landau [36]. For $T \gtrsim 171$ MeV the order parameter u tends to zero and is a multi-valued function of ρ_B, the phase transition is found to be first-order when applying to these regions the method of Ref. [2] which essentially identifies the multi-valued region of the order parameter to the region of a first-order phase transition. It is the chiral phase transition displayed on the phase diagram of Fig. 3. The dashed line denotes a second-order phase transition, ending up with a tricritical point, CP ($T \simeq 171$ MeV, $\mu_B \simeq 980$ MeV), signaling the onset of a first-order phase transition. This is evidenced from the evolution of the effective potential as a function of M^* for several values of T belonging to the multivalued regions of the chiral condensate (Fig. 8).

From Figs. 2, 7, and 8 it is evident that the restoration of chiral symmetry occurs for $T = 0$ at the critical density $\rho_c \simeq 2.2\rho_0$, and that the second-order transition is associated with a minimum of the effective potential. As T increases, this minimum splits out into two minima at $T \simeq 171$ MeV with a

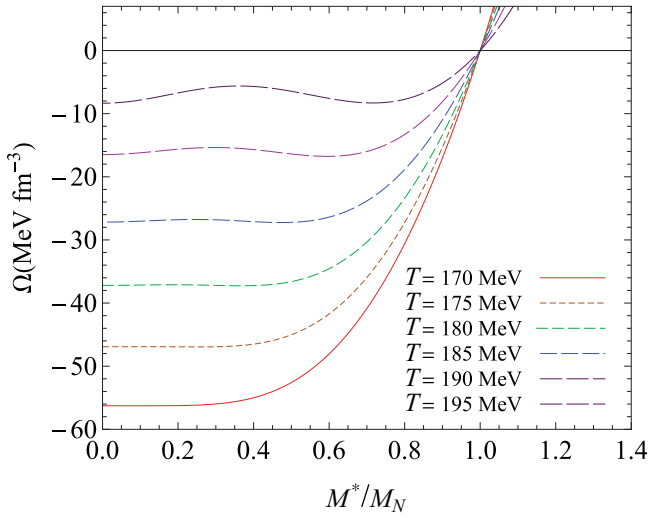

FIG. 8. (Color online) The evolution of effective potential vs M^* at several values of T and μ_B in the region of chiral phase transition.

barrier in-between signaling the onset of a first-order phase transition. The second-order chiral transition in the region ($0 \leqslant T \lesssim 171$ MeV, $980 \lesssim \mu_B \lesssim 1210$ MeV) is visible on the evolution of the chiral condensate as a function of T for several values of μ_B in the region $980 \lesssim \mu_B \lesssim 1210$ MeV (Fig. 9).

Thus, while the liquid-gas transition occurs at saturation density, the chiral transition occurs at higher density. The direct signature of chiral symmetry restoration is the vanishing chiral condensate associated with the zero of $u(T, \mu_B)$. This is illustrated in Fig. 3 where the solid lines denote the first-order chiral restoration phase transition and the dashed line denotes the second-order chiral restoration phase transition, which are separated by a tricritical point. We can therefore conclude that there are really two types of phase diagrams for this model: a first-order liquid-gas phase transition of nuclear matter occurring at saturation density, and a chiral phase transition with two types of phase order, separated by a tricritical point.

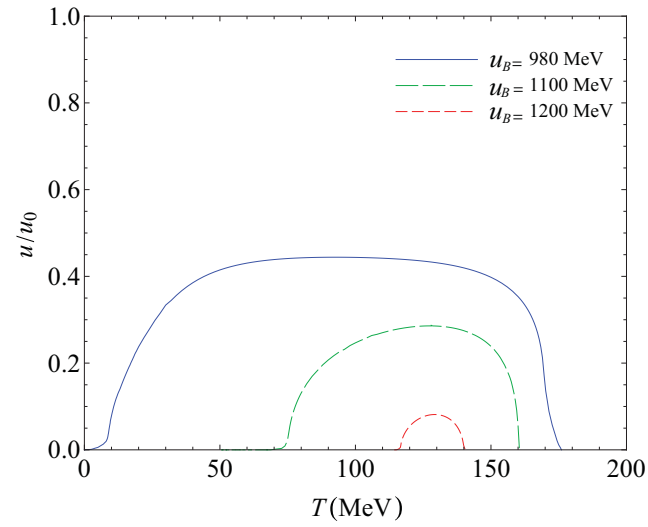

FIG. 9. (Color online) The evolution of the chiral condensate versus T for several values of μ_B in the region $980 \lesssim \mu_B \lesssim 1210$ MeV.

V. CONCLUSION AND OUTLOOK

We have presented a systematic study of phase transitions in chiral nuclear matter as described by the ENJL model including additional scalar-vector interaction terms. We formulate the model in terms of nucleonic degrees of freedom bearing in mind that normal nuclei are indeed made of nucleons. The main results are summarized below.

(i) The model is able to reproduce well-observed saturation properties of nuclear matter such as equilibrium density, binding energy, compression modulus, and nucleon effective mass at the saturation density $\rho_B = \rho_0$. The best fit of nuclear properties is achieved with the cutoff momentum $\Lambda = 0.4$ GeV which is noticeably smaller than usually assumed for quark-based models, with an indication that using nucleonic quasi-particles is justified at low momenta in the nuclear medium.

(ii) The model predicts two interesting features. First, it reveals a first-order phase transition of the liquid-gas type occurring at subsaturated densities, starting from $T = 0$, $\mu_B \simeq 923$ MeV and extending to a crossover critical end point CEP at $T \simeq 18$ MeV, $\mu_B \simeq 922$ MeV. This phenomenon is also apparent from the evolution of the effective potential as a function of effective nucleon mass, the equation of state, and the dependence of the scalar density (and effective nucleon mass) on μ_B.

(iii) The model predicts in addition an exact restoration of chiral symmetry at high baryon densities, $\rho_B \gtrsim 2.2\rho_0$ for $0 \lesssim T \lesssim 171$ MeV and $\mu_B \gtrsim 980$ MeV, and $\rho_B \lesssim 2.2\rho_0$ for $T \gtrsim 171$ MeV. In the (T, μ_B) plane a second-order chiral phase transition occurs at $T = 0$, $\mu_B \simeq 980$ MeV and extends to a tricritical point CP at $T \simeq 171$ MeV, $\mu_B \simeq 980$ MeV, signaling the onset of a first-order phase transition. This phenomenon is also apparent from the evolution of the effective potential as a function of effective nucleon mass and T dependence of chiral condensate for $\mu_B \gtrsim 980$ MeV.

It is important to stress that our model is able to describe simultaneously the saturation properties of nuclear matter at normal density and the restoration of chiral symmetry at high baryon densities. It exhibits one first-order phase transition of the liquid-gas type at subsaturation densities exclusively. Restoration of chiral symmetry develops gradually with increasing baryon density and leads to two types of phase transition orders. There exists a triple (tricritical) point in the (T, μ_B) plane where the line of first-order chiral phase transition meets the line of second-order phase transition. Since the order of chiral transition plays a significant role in the dynamical evolution of the system [40] it is interesting to investigate the physical properties of the system in regions of different orders of transitions. The phase structure of the chiral phase transition obtained in the present work is expected to share some features with that derived from lattice calculations and effective quark models.

The chiral phase diagram obtained here differs from that obtained on the lattice (more or less quark masses) in the chiral limit and for $N_f = 2$ quark flavors: a crossover transition at high T and low μ_B becomes a second order transition [43]. However, this situation resembles very closely that obtained in lattice QCD calculations in the limit of "heavy" quark masses and in the strong-coupling limit, where one finds a first-order transition at high T and low μ_B [44,45]. Such a feature is also found in Walecka's model for some choices of the parameters [42].

QCD simulations have suggested that the chiral phase transition is accompanied by a deconfinement transition at the same critical temperature T_c [41]. Our calculation gives $T_c \simeq 171$ MeV at $\mu_B \simeq 980$ MeV, in good agreement with the lattice QCD simulation, which suggests $T_c = 140$–190 MeV [41] and predicts a chiral-deconfinement transition at temperatures of the order of 170 MeV [4].

In conclusion, for the first time, we have obtained a good description of hot and dense nuclear matter on the basis of a relatively simple chiral model. Within this model, normal nuclei are interpreted as droplets of baryon-rich matter in a phase with spontaneously broken chiral symmetry. The approach to a phase with restored chiral symmetry is predicted at baryon densities above $2\rho_0$. The chiral transition in baryon-rich matter is clear. We believe that effects of the chiral symmetry restoration will be most clearly seen in nuclear collisions at energies of a few $10A$ GeV, where highest baryon densities are expected.

Finally, owing to the fact that the ENJL model satisfactorily reproduces all basic static properties of nuclear matter and predicts an exact chiral transition, it might be a good candidate for theoretically exploring the in-medium dynamics of hadrons, such as kaon and pion condensation in dense matter. Moreover, the model can be easily extended to asymmetric matter and finite nuclei.

ACKNOWLEDGMENTS

The authors are grateful to Professor Tran Huu Phat for useful suggestions and thank Professor Darriulate Pierre for reading the manuscript and giving valuable comments. D.T.T. would like to express his sincere thanks to the Vietnam Atomic Energy Commission for the hospitality extended to him during his Ph.D. study. This paper is financially supported by the Vietnam National Foundation for Science and Technology Development (NAFOSTED).

[1] J. B. Kogut, D. Toublan, and D. K. Sinclair, Phys. Lett. B **514**, 77 (2001); S. Hands, S. Kim, and J. I. Skullerud, Phys. Rev. D **81**, 091502(R) (2010).
[2] M. Askawa and K. Yazaki, Nucl. Phys. A **504**, 668 (1989).
[3] O. Scavenius, A. Mocsy, I. N. Mishustin, and D. H. Rischke, Phys. Rev. C **64**, 045202 (2001); J. Andersen and L. Kyllingstad, J. Phys. G **37**, 015003 (2010).
[4] F. Karsch, Nucl. Phys. A **698**, 199 (2002).
[5] H. Muller and B. D. Serot, Phys. Rev. C **52**, 2072 (1995).
[6] V. Baran, M. Colonna, M. Di Toro, and A. B. Larionov, Nucl. Phys. A **632**, 287 (1998).
[7] C. Ducoin, Ph. Chomaz, and F. Gulminellei, Nucl. Phys. A **771**, 68 (2006).
[8] G. Torrieri and I. Mishustin, Phys. Rev. C **82**, 055202 (2010).
[9] M. Jin, M. Urban, and P. Schuck, Phys. Rev. C **82**, 024911 (2010).
[10] A. Rios, Nucl. Phys. A **845**, 58 (2010).
[11] A. Rios, A. Polls, A. Ramos, and H. Muther, Phys. Rev. C **78**, 044314 (2008).
[12] G. Chaudhuri and S. DasGupta, Phys. Rev. C **80**, 044609 (2009).
[13] W. Weise, Prog. Theor. Phys. Suppl. **186**, 390 (2010).
[14] I. N. Mishustin, L. M. Satarov, and W. Greiner, Phys. Rep. **391**, 363 (2004).
[15] Y. Tsue, J. da Providencia, C. Providencia, and M. Yamamura, Prog. Theor. Phys. **123**, 1013 (2010).
[16] D. B. Serot and J. D. Walecka, in *Advanced Nuclear Physics*, edited by J. W. Negele and E. Vogt (Plenum Press, New York, 1986), Vol. 16, p. 1.
[17] Y. Nambu and G. Jona-Lasinio, Phys. Rev. **122**, 345 (1961); **124**, 246 (1961).
[18] M. Gell-Mann and M. Levy, Nuovo Cimento **16**, 705 (1960).
[19] T. D. Lee and G. C. Wick, Phys. Rev. D **9**, 2291 (1974).
[20] J. Boguta, Phys. Lett. B **120**, 34 (1983).
[21] I. N. Mishustin, J. Bondorf, and M. Rho, Nucl. Phys. A **555**, 215 (1993).
[22] G. W. Carter and P. J. Ellis, Nucl. Phys. A **628**, 325 (1998).
[23] P. Papazoglou, S. Schramm, J. Schaffner-Bielich, H. Stöcker, and W. Greiner, Phys. Rev. C **57**, 2576 (1998).
[24] P. Papazoglou, D. Zschiesche, S. Schramm, J. Schaffner-Bielich, H. Stöcker, and W. Greiner, Phys. Rev. C **59**, 411 (1999).
[25] V. Koch, T. S. Biro, J. Kunz, and U. Mosel, Phys. Lett. B **185**, 1 (1987).
[26] M. Buballa, Nucl. Phys. A **611**, 393 (1996).
[27] I. N. Mishustin, in *Proceedings of the International Conference on Nuclear Physics at the Turn of Millenium*, Wilderness, 1996, edited by H. Stöcker, A. Gallman, and J. H. Hamilton (World Scientific, Singapore, 1997), p. 499.
[28] Tran Huu Phat, Nguyen Tuan Anh, and Dinh Thanh Tam, Phys. Rev. C **84**, 024321 (2011).
[29] N. K. Glendenning, Phys. Rev. C **37**, 2733 (1988).
[30] B. Friedman and V. R. Pandharipande, Nucl. Phys. A **361**, 502 (1981).
[31] M. M. Sharma, W. T. A. Borghols, S. Brandenburg, S. Crona, A. van der Woude, and M. N. Harakeh, Phys. Rev. C **38**, 2562 (1988).
[32] K. Fukushima and T. Hatsuda, Rep. Prog. Phys. **74**, 014001 (2011).
[33] P. Chomaz, arXiv:nucl-ex/0410024.
[34] H. R. Jaqaman, A. Z. Mekjian, and L. Zamick, Phys. Rev. C **27**, 2782 (1983); **29**, 2067 (1984).
[35] L. P. Czernai *et al.*, Phys. Rep. **131**, 223 (1986).
[36] L. D. Landau and E. M. Lifshitz, *Statistical Physics* (Pergamon, New York, 1969).
[37] B. Borderie *et al.*, Prog. Part. Nucl. Phys. **61**, 557 (2008).

[38] P. Danielewicz, R. Lacey, and W. G. Lynch, Science **298**, 1592 (2002).
[39] M. Buballa, Phys. Rep. **407**, 205 (2005).
[40] D. H. Rischke and M. Gyulassy, Nucl. Phys. A **608**, 479 (1996); I. N. Mishustin, Phys. Rev. Lett. **82**, 4779 (1999); I. N. Mishustin and O. Scavenius, *ibid.* **83**, 3134 (1999).
[41] J. Wambach, arxiv:1101.4760.
[42] J. Theis, G. Graebner, G. Buchwald, J. Maruhn, W. Greiner, H. Stocker, and J. Polonyi, Phys. Rev. D **28**, 2286 (1983).
[43] O. Philipsen, arXiv:1111.5370.
[44] M. Fromm, J. Langelage, S. Lottini, and O. Philipsen, arXiv:1111.4953.
[45] K. Miura, T. Z. Nakano, A. Ohnishi, and N. Kawamoto, PoS Lattice **2010**, 202 (2010).